Robotica (2006) volume 24, pp. 229–237. © 2005 Cambridge University Press
doi:10.1017/S0263574705002067 Printed in the United Kingdom

Modeling and control of a new robotic deburring system

Jae H. Chung* and Changhoon Kim

Department of Mechanical Engineering, Stevens Institute of Technology, Castle Point on Hudson, Hoboken, N. J. 07030 (USA)

(Received in Final Form: April 27, 2005, first published online 31 October 2005)

SUMMARY

This paper discusses the modeling and control of a robotic manipulator with a new deburring tool, which integrates two pneumatic actuators to take advantage of a double cutting action. A coordination control method is developed by decomposing the robotic deburring system into two subsystems; the arm and the deburring tool. A decentralized control approach is pursued, in which suitable controllers were designed for the two subsystems in the coordination scheme. In simulation, three different tool configurations are considered: rigid, single pneumatic and integrated pneumatic tools. A comparative study is performed to investigate the deburring performance of the deburring arm with the different tools. Simulation results show that the developed robotic deburring system significantly improves the accuracy of the deburring operation.

KEYWORDS: Deburring system; Different tools; Double cutting action.

I. INTRODUCTION

A machining manipulator is subject to mechanical interaction with the object being processed. The robot performs the task in constrained work space. In constrained tasks, one is concerned with not only the position of the robot end-point, but also the contact forces, which are desired to be accommodated rather than resisted. Therefore, the interaction force needs to be considered in designing and controlling deburring tools.

Many researchers have proposed automated systems for grinding dies, deburring casting, removing weld beans, etc.[1,2] Usually, a deburring tool is mounted on a NC machining center or a robot manipulator. Several control laws have been developed for simultaneous control of both motion and force[3–5] of robotic manipulators. Despite the diversity of approaches, it is possible to classify most of the control methods into two major approaches: impedance control[6–8] and hybrid position/force control.[9–12] However, these methods require an accurate model of force interaction between the manipulator and the environment and are difficult to implement on typical industrial manipulators that are designed for position control.

An active feedback control scheme was developed in order to supply compliance for robotic deburring as a means to accommodate the interaction force due to contact motion. Kuntze[13,14] suggested an active control scheme, in which the actuators are commanded to increase torques in the opposite direction of the deflections. Paul[15]applied an active isolator to a chipping robot, where the isolator attached to the arm tip reduces the vibration seen by the robot. Sharon and Hardt[16] developed a multi-axis local actuator, which compensates for positioning errors at the end point, in a limited range.

Asada and West[17–20] developed passive tool support mechanisms, which couple the arm tip to the workpiece surface and bear large vibratory loads. These mechanisms allow the robot to compensate for the excessive deflection when the robot contacts the workpiece. These methods reduce dynamic deflection in a certain frequency range. However, it is difficult for these control schemes, which are employed for a robot with a passive tool, to perform well over a wide frequency band because they must drive the entire, massive robot arm. In addition, unknown compliance from a passive tool makes it difficult to control the deburring robot.

In this paper, a robotic deburring method is developed based on an integrated pneumatic actuation system (IPAS), which considers the interaction among the tool, the manipulator, and the workpiece and couples the tool dynamics and a control design that explicitly considers deburring process information. First, a mathematical model of a single pneumatic actuator is developed. Then, a new active tool is developed based on two pneumatic actuators, which utilizes double cutting action – initial cut followed by fine cut. Then, a coordination based control method is developed for the robotic deburring system based on the active pneumatic deburring tool, which utilizes coordination of two cutters. Simulation results show that the developed system significantly reduces the chattering of the deburring robot and improves the accuracy of the deburring operation.

II. MODELING OF THE DEBURRING ROBOT

In this section, a dynamic model of a robotic arm with the new deburring tool or IPAS is developed as a robotic deburring system. The load dynamics of a single pneumatic actuator is described and utilized for developing a dynamic model of the IPAS, which integrates two pneumatic cylinders. Then, the equations of motion of the deburring robot are derived.

II.1. Single pneumatic actuator

The single pneumatic tool is illustrated in Figure 1, where $i = 1, 2$, G_i is the entering mass flow, P_i is the chamber

* Corresponding author.

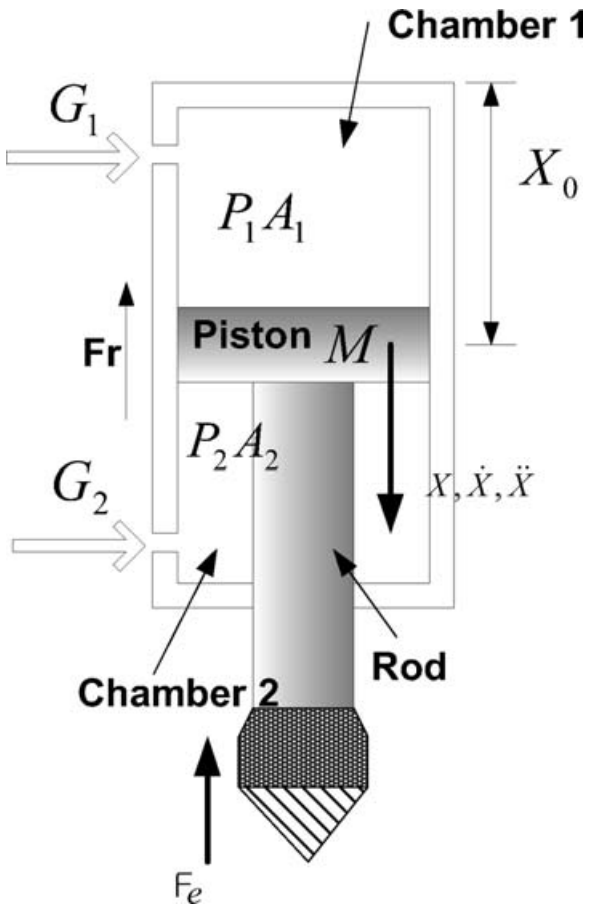

Fig. 1. Pneumatic tool.

pressure, V_i is the volume of the chamber, X, $\dot{X}$and $\ddot{X}$ are the position, velocity and acceleration of the piston, respectively, A_i, M, and X_0 are the area, the mass, the initial position of the piston, respectively, F_e and F_r are the external and friction forces, respectively.

The chamber pressure and the kinetic variables are related by the equilibrium equation[21–23]

$$G_i = \rho_i \frac{dV_i}{dt} + V_i \frac{d\rho_i}{dt} \quad (i = 1, 2) \tag{1}$$

where G_i is the entering mass flow, ρ_i the air density and V_i the volume of the Chamber i. The air is assumed to be ideal gas, which can be written as

$$\rho_i = \rho_{ij}\left(\frac{P_i}{P_{ij}}\right)^{1/n} = \frac{P_{ij}}{RT_{ij}}\left(\frac{P_i}{P_{ij}}\right)^{1/n} \tag{2}$$

where the subscript j denotes the initial conditions, R the air constant, P the air pressure in the cylinder, and T the absolute air temperature. According to the displacement of the piston rod, the volume of the chambers is written as

$$V_i = A_i(X_0 \pm X) \tag{3}$$

where the subscripts 0 indicates the initial position of piston M, respectively, and A_i denotes the area of the piston. By combining Eqs. (2) and (3) and their time derivative in Eq. (1), the following expression is obtained:

$$G_i = A_i(X_0 \pm X)\frac{1}{nRT_{ij}}\left(\frac{P_i}{P_{ij}}\right)^{1/n-1}\frac{dP_i}{dt} \pm \frac{P_{ij}}{RT_{ij}}\left(\frac{P_i}{P_{ij}}\right)^{1/n} A_i \frac{dx}{dt}. \tag{4}$$

Eq. (4) can be rewritten as

$$\frac{dP_i}{dt} = \frac{nRT_{ij}}{A_i(X_0 \pm X)(P/P_{ij})^{1/n-1}} G_i \mp \frac{nP_i}{(X_0 \pm X)}\frac{dx}{dt}. \tag{5}$$

The load dynamics can be written for the system as following:

$$A_1P_1 - A_2P_2 - K_f\dot{X} = M\ddot{X} + F_e \tag{6}$$

where $\dot{X}$ and $\ddot{X}$ represent the velocity and acceleration of the piston, respectively, K_f and F_e are the viscous friction coefficient and the external force exerted on the piston,[9,11] respectively, and M denotes the mass of each piston.

II.2. Integrated pneumatic actuation system (IPAS)

Figure 2 shows the integrated cylinder, which is comprised of three chambers and actuated by a single valve connected to Chamber 3. Note that the IPAS is a single input system with two pistons. The pistons are not directly connected to the inner pistons, M_3 and M_4, which create a unique configuration of three chambers connected in series. This configuration allows the chambers adjacent to the active chamber to act as vibration isolators. This feature enables the IPAS to damp out the chatter caused by external loads and air compressibility. Therefore, double cutting action and chattering reduction can be achieved simultaneously.

According to the variable volumes of the chambers, the changing dynamic relationship can be represented by the following equation:[10]

$$G_3 = \rho_3 \frac{dV_3}{dt} + V_3 \frac{d\rho_3}{dt} \tag{7}$$

where G_3 is the entering air flow, ρ_3 the air density and V_3 the volume of Chamber 3. It is assumed that the condition of the air is ideal as following:

$$\rho_3 = \rho_{3j}\left(\frac{P_3}{P_{3j}}\right)^{1/n} = \frac{P_{3j}}{RT_{3j}}\left(\frac{P_3}{P_{3j}}\right)^{1/n} \tag{8}$$

where the subscript j indicates the initial conditions and n is the air transformation ratio. Now, V_3 is derived as

$$V_3 = A_3(L - X_4 - X_3) \tag{9}$$

where A_3 denotes the area of Piston 3, and X_i $(i = 4, 3)$ is the position of Piston i. L denotes the length of Chamber 3 as shown in Figure 3. By combining Eqs. (8) and (9) and their time derivatives in Eq. (7), the following expression is

https://doi.org/10.1017/S0263574705002067 Published online by Cambridge University Press

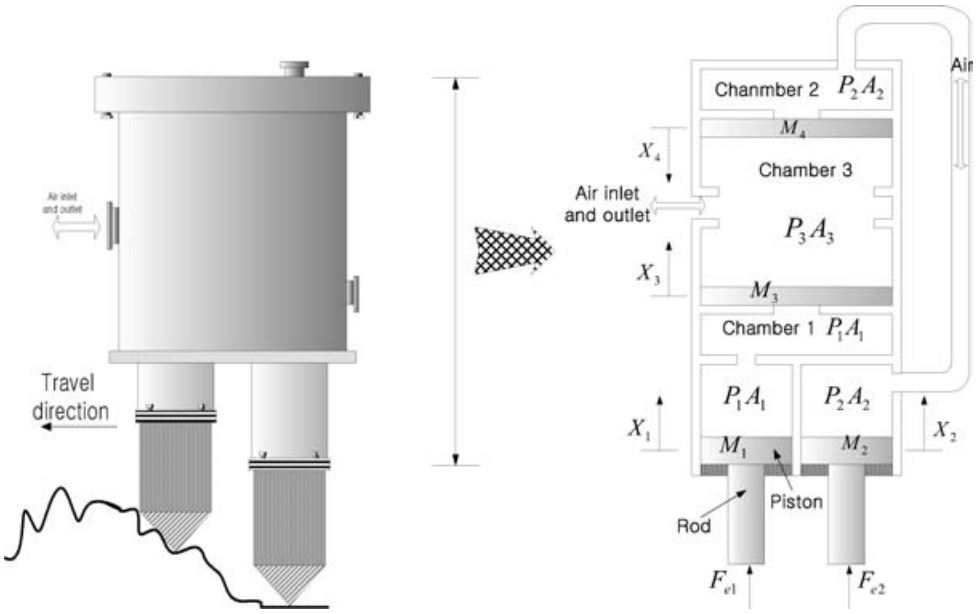

Fig. 2. Integrated double cylinder system.

be obtained:

$$G_3 = A_3(L - X_4 - X_3)\frac{1}{nRT_{3i}}\left(\frac{P_3}{P_{3i}}\right)^{1/n-1}\frac{dP_3}{dt} + \frac{P_{3i}}{RT_{3i}}\left(\frac{P_3}{P_{3i}}\right)^{1/n}A_3\frac{dx}{dt}. \quad (10)$$

Then, the pressure gradient is be written as

$$\frac{dP_3}{dt} = \frac{nRT_{3i}}{A_3(L - X_4 - X_3)(P_3/P_{3i})^{1/n-1}}G_3 - \frac{nP_3}{(L - X_4 - X_3)}\frac{dx}{dt}. \quad (11)$$

Now, the load dynamics of the integrated system is considered as following:

$$-K(X_1 - X_3) - C(\dot{X}_1 - \dot{X}_3) + M_1\ddot{X}_1 + F_{e1} - F_{f1} = 0 \quad (12)$$

and

$$-K(X_2 - X_4) - C(\dot{X}_2 - \dot{X}_4) + M_2\ddot{X}_2 + F_{e2} - F_{f2} = 0 \quad (13)$$

where $\dot{X}_i$ and $\ddot{X}_i$ represent the velocity and the acceleration of each piston. F_{fi} denotes the viscous friction force of the piston rod ($i = 1, 2, 3, 4$), F_{ei} is the external force ($i = 1, 2$), and P_i and A_i denote the air pressure and the area of the piston, respectively. Then the dynamic equations are written as

$$K(X_1 - X_3) + C(\dot{X}_1 - \dot{X}_3) + M_3\ddot{X}_3 = P_3A_3 - F_{f3} \quad (14)$$

and

$$K(X_1 - X_4) + C(\dot{X}_1 - \dot{X}_4) + M_4\ddot{X}_4 = P_3A_3 - F_{f4} \quad (15)$$

where K and C are stiffness and damping coefficients of the system, respectively.

II.3. Robotic deburring system

Figure 3 illustrates a three-link rigid robot with the pneumatic deburring tool described earlier. Using the well-known Lagrangian equations, the following equations of motion of the deburring robot were obtained:

$$\bar{m}(q)\ddot{q} + \bar{c}(q, \dot{q})\dot{q} + \bar{g}(q) = \tau \quad (16)$$

where q, $\dot{q}$, $\ddot{q}$ are the joint angle, the joint angular velocity, and the joint angular acceleration, respectively, $\bar{m}(q)$ is the 3×3 symmetric positive-definite inertia matrix, $\bar{c}(q, \dot{q})\dot{q}$ is

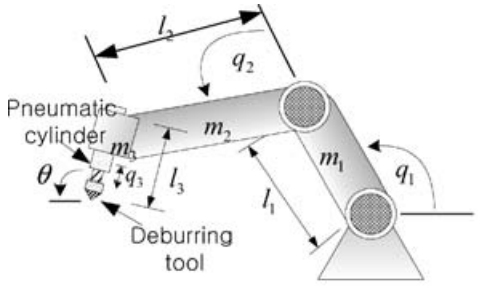

m_i : Mass of each link

l_i : Length of each link

q_i : Each joint angle and displacement

θ : Contact angle $(i = 1,2,3)$

Fig. 3. Deburring robot with pneumatic tool.

https://doi.org/10.1017/S0263574705002067 Published online by Cambridge University Press

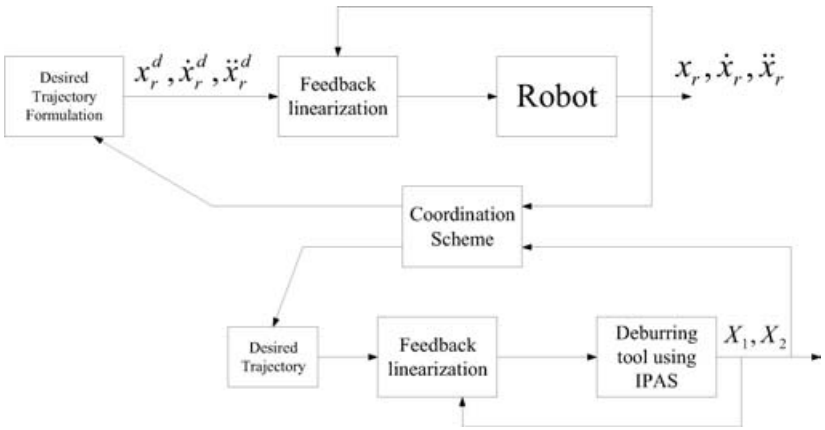

Fig. 4. Block diagram for coordinated control for robotic deburring.

the 3×1 vector of Coriolis and centrifugal torques, $\bar{g}(q)$ is the 3×1 gravitational torques, and τ is the 3×1 vector of the joint torques.

The mass of the links and pneumatic cylinder are considered as if they were rigidly attached. The relationship between the joint and the tip velocities can be written as

$$\dot{x} = J(q)\dot{q} \tag{17}$$

where $J(q)$ is the geometric Jacobian of the manipulator. By differentiating Eq. (17), the Cartesian acceleration term can be found as

$$\ddot{x} = J(q)\ddot{q} + \dot{J}\dot{q}. \tag{18}$$

Now, Eq. (16) is rewritten as

$$\ddot{q} = \overline{m}^{-1}(q)(\tau - \bar{c}(q, \dot{q}) - \bar{g}(q)) \tag{19}$$

from Eq. (18) and suppressing arguments for brevity, the following equation is obtained

$$\ddot{x} = \overline{Jm}^{-1}(\tau - \bar{c}(q, \dot{q}) - \bar{g}(q)) + \dot{J}\dot{q}. \tag{20}$$

Then, the equations of motion of the robot are obtained as following:

$$m(x)\ddot{x} + c(x, \dot{x}) + g(x) = f \tag{21}$$

where $f = (J^T)^{-1}\tau$ is input expressed in task space.

Let the dynamic equation of the robot manipulator in the constraint coordinates be represented as

$$m(x)\ddot{x} + c(x, \dot{x})\dot{x} + g(x) = f + f_{rf}. \tag{22}$$

where f denotes the input force and f_{rf} is the resultant force of the normal force f_n and the tangential force f_t exerted on the tool tip. The tangential force [9,10,19] can be represented as

$$f_t = \frac{bdv_t e_m}{V_t} \tag{23}$$

where V_t is the spindle speed of deburring tool; b is the tool width; d is the depth of cut; v_t is the feed rate (or the traveling speed of the end effector along the surface of the workpiece); e_m is the material-stiffness of the workpiece. The normal force f_n is assumed to be proportional to the tangential force f_t. Besides, the force angle of the deburring tool affects the tangential force. Although the value of the angle may vary substantially depending on the nature of the material flow at the tool-chip interface, as approximation 0.3 was used in these calculations.[12] Therefore, the normal force f_n is considered to be smaller than the tangential force f_t in Eq (23), where the ratio is $f_n/f_t \approx 0.3$.[24]

III. CONTROL DESIGN

The IPAS based deburring robot can be treated as a system that consists of two primary subsystems; the arm and the IPAS. The two subsystems differ substantially in their task assignments, dynamic characteristics and controller requirements. This physical interpretation provides an efficient approach to the control of the robotic deburring system. The control strategy for the deburring robot is illustrated in Figure 4. The arm is commanded to follow the desired trajectory in task space, which is modified based on the position of the second piston due to varying length of the tool. In other words, the primary cutter at the front side cuts the burr first and the second cutter then attempts to eliminate the remaining burr. In case that the burr is not removed completely, the uncut depth is incorporated into the desired trajectory for compensation.

The developed control design is a decentralized control,[25–27] which consists of two independent controllers interacting based on the coordination scheme aforementioned for the manipulator and the IPAS, respectively. Constraint equations are derived in terms of position variables and are differentiated twice to lead to a relationship in terms accelerations, which integrate the separate controllers for stability proof. Feedback linearization is employed to design a coordination based controller. In what follows, it is shown that use of a nonlinear dynamic feedback achieves exact linearization and input-output decoupling for the robotic deburring system.

The coordination control method is developed first and then its efficiency will be compared with the hybrid control method through simulation study.

https://doi.org/10.1017/S0263574705002067 Published online by Cambridge University Press

III.1. Coordination control

The decoupled dynamic robot model become as following:

$$m_r(x_r)\ddot{x}_r + c_r(x_r, \dot{x}_r) = f_r - R_r(x_r)\ddot{X}_t \tag{24}$$

where x_r, $\dot{x}_r$ and $\ddot{x}_r$ denote the displacement, velocity and acceleration of the tip of the manipulator, m_r is the inertia mass matrix, c_r consists of Coriolis, centripetal, and gravity forces, f_r is the input force acting on the tip of the mainpulator, $R_r$is the inertia matrix which reflects the dynamic effect of the deburring tool on the manipulator, and $\ddot{X}_t$ is the acceleration of IPAS. Likewise, the equations of motion for deburring tool are written as

$$M_t\ddot{X}_t - C_t(\dot{X}_j) + F_e = F_t(A_3, P_3) - R_t(x_r)\ddot{x}_r \tag{25}$$

where $\ddot{X}_t$ and $\dot{X}_t$ denote the acceleration and velocity of each piston, M_t is the mass matrix, C_t consists of the viscous friction and gravity forces, F_t is the forces acting on the pistons, R_t is the inertia matrix which represents the end point of the manipulator on the tool, F_e is the external force of IPAS. Let p denote the position vector of the contact point, in fixed workspace coordinate system. Therefore the robotic deburring system is assumed that the constraint surface can be defined in algebraic terms by

$$\phi(p) = 0 \tag{26}$$

where p is comprised of x_r and X_t. Now, the constraint equation (26) is differentiated once as following:

$$\dot{\phi}(p) = J_c(q)\dot{q} = 0 \tag{27}$$

where J_c denotes the geometric Jacobian matrix. The initial Lagrange coordinate q_0 satisfies the holonomic constraint $\phi(p_0) = 0$, where p_0 is the initial position of the robot. Then, Eq. (27) is differentiated once to produce $\ddot{\phi} = 0$, into which the subsystems, Eqs. (24) and (25) are incorporated. Then, feedback linearization can be applied to cancel the coupling terms and to design linear controllers as the outer feedback loop. Since the manipulator velocity is always in the null space of $\dot{\phi}(p)$, it is possible to define a vector of generalized velocities $\eta(t)$ as following:

$$\dot{x}_r = \zeta(x_r)\eta(t) \tag{28}$$

where $\zeta(x_r)$is a full matrix, whose columns are in the null space of $\phi(p)$. Differentiating (28), substituting the resulting expression for $\ddot{x}_r$into Eq. (24), and premultiplying Eq. (24) by ζ^T, we have

$$\zeta^T(m_r\zeta\dot{\eta} + m_r\dot{\zeta}\eta + c_r) = \zeta^T f_r - \zeta^T R_r\ddot{X}_t. \tag{29}$$

Note that $\zeta^T\phi^T = 0$.

Similarly substituting $\ddot{x}_r$into Eq. (25), we have

$$M_t\ddot{X}_t - C_t + F_e = F_t - R_t\dot{\zeta}\eta - R_t\zeta\dot{\eta}. \tag{30}$$

Using the state vector $\chi = [\,x_r^T\ X_t^T\ \eta^T\ \dot{X}_t^T\,]^T$ and the block partition of the state vector

$$\chi = \begin{bmatrix}\chi_1\\ \chi_2\\ \chi_3\end{bmatrix}, \quad \text{with } \chi_1 = x_r,\ \chi_2 = X_t,\ \chi_3 = \begin{bmatrix}\eta\\ \dot{X}_t\end{bmatrix}.$$

Where $X_t = [X_1, X_2]$ is the displacement of each position.

The following expression is obtained:

$$\dot{\chi} = \begin{bmatrix}\dot{\chi}_1\\ \dot{\chi}_2\\ \dot{\chi}_3\end{bmatrix} = \begin{bmatrix}\zeta\eta\\ \dot{X}_t\\ M^{-1}C\end{bmatrix} + \begin{bmatrix}0\\ 0\\ M^{-1}E\end{bmatrix}\lambda \tag{31}$$

where

$$M = \begin{bmatrix}\zeta^T m_r\zeta & \zeta^T R_r\\ R_t\zeta & M_t\end{bmatrix}, \quad E = \begin{bmatrix}\zeta^T & 0\\ 0 & I\end{bmatrix},$$

$$C = \begin{bmatrix}-\zeta^T m_r\dot{\zeta}\eta & -\zeta^T c_r\\ C_t + F_e & -R_t\dot{\zeta}\eta\end{bmatrix}, \quad \text{and} \quad \lambda = \begin{bmatrix}f_r\\ F_t\end{bmatrix}.$$

The system is input-output linearizable by using the following nonlinear feedback:

$$\lambda = E^{-1}(Mu - C), \tag{32}$$

which results in simpler state equations as following:

$$\dot{\chi} = \begin{bmatrix}\zeta\eta\\ \dot{X}_t\\ 0\end{bmatrix} + \begin{bmatrix}0\\ 0\\ I\end{bmatrix}u. \tag{33}$$

To derive the decoupling matrix, each component of the output equations is differentiated until the input appears explicitly in the derivative. In this case, the output equation is differentiated twice as following:

$$y = \begin{bmatrix}f_1\\ f_2\end{bmatrix} \tag{34}$$

$$\ddot{y} = \dot{\Phi}(\chi)\begin{bmatrix}\eta\\ \dot{X}_t\end{bmatrix} + \Phi(\chi)u \tag{35}$$

where $\Phi(\chi)$ is the decoupling matrix of the system given by

$$\Phi(\chi) = \begin{bmatrix}\Phi_r(\chi) & 0\\ 0 & \Phi_t(\chi)\end{bmatrix} \tag{36}$$

where

$$\Phi_p(\chi) = \frac{\partial f_1(X_t)}{\partial X_t}, \quad f_1 = X_t + f_2$$

$$\Phi_r(\chi) = \frac{\partial f_2(q_r)}{\partial q_r}, \quad f_2(q_r) = \begin{bmatrix}l_1\cos q_1 + l_2\cos(q_1 + q_2)\\ l_1\sin q_1 + l_2\sin(q_1 + q_2)\end{bmatrix}$$

Applying the following nonlinear state feedback

$$u = \Phi^{-1}(\chi)\left(\upsilon - \dot{\Phi}(\chi)\begin{bmatrix}\eta\\ \dot{X}_t\end{bmatrix}\right), \tag{37}$$

the input-output relationship is decoupled because each component of the auxiliary input, υ, controls one and only one component of the output, y. It is noted that the existence of the nonlinear feedback require the inverse of the decoupling matrix$\Phi(\chi)$. To complete the controller design,

https://doi.org/10.1017/S0263574705002067 Published online by Cambridge University Press

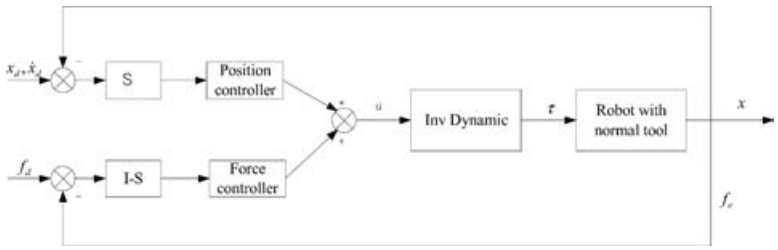

Fig. 5. Block diagram for Robot with deburring tool (Hybrid control)

it is necessary to stabilize each of the above subsystem with constant state feedback. Then, the stability of the system is guaranteed by selecting appropriate constant feedback gains for the linearized system.

III.2. Hybrid control of the robot with a rigid tool

The robotic arm with a rigid tool is considered for the hybrid control design. The performance of the active pneumatic tool based deburring can be degraded due to the fact that the hybrid control method explicitly controls the position and force simultaneously, which can be difficult for a compliant tool.

Since a manipulator task specification, such as deburring a work-piece is typically given relative to the end-effector, the dynamic equation is represented in task space, rather than joint space or actuator space. The controller is designed by considering these coordinates, whose control input τcan be transformed to the torque in the joint coordinates. The transformation is

$$\tau = J^T(x)u_h. \tag{38}$$

In the constraint coordinates, the force and position errors are defined. $f_{di} \in R^1$ is the desired force in the x_i direction $(i = 1, 2)$ and $x_{id} \in R^{n-1}$ is the desired position in other directions. From the assumption that the stiffness k_e is known, e_p is defined as

$$e_p = K^{-1}\begin{pmatrix} e_f \\ e_{p2} \end{pmatrix} = K^{-1}\begin{pmatrix} f_{d1} - f_1 \\ x_{2d} - x_2 \end{pmatrix} \tag{39}$$

where $k = \begin{pmatrix} k_e & 0 \\ 0 & I \end{pmatrix}$. x_i is the displacement of the robot, x_{id} the desired position , and $f_i \in R^1$ the force component of the x_i direction. Figure 5 depicts hybrid control of a robot with a rigid tool without a pneumatic cylinder.

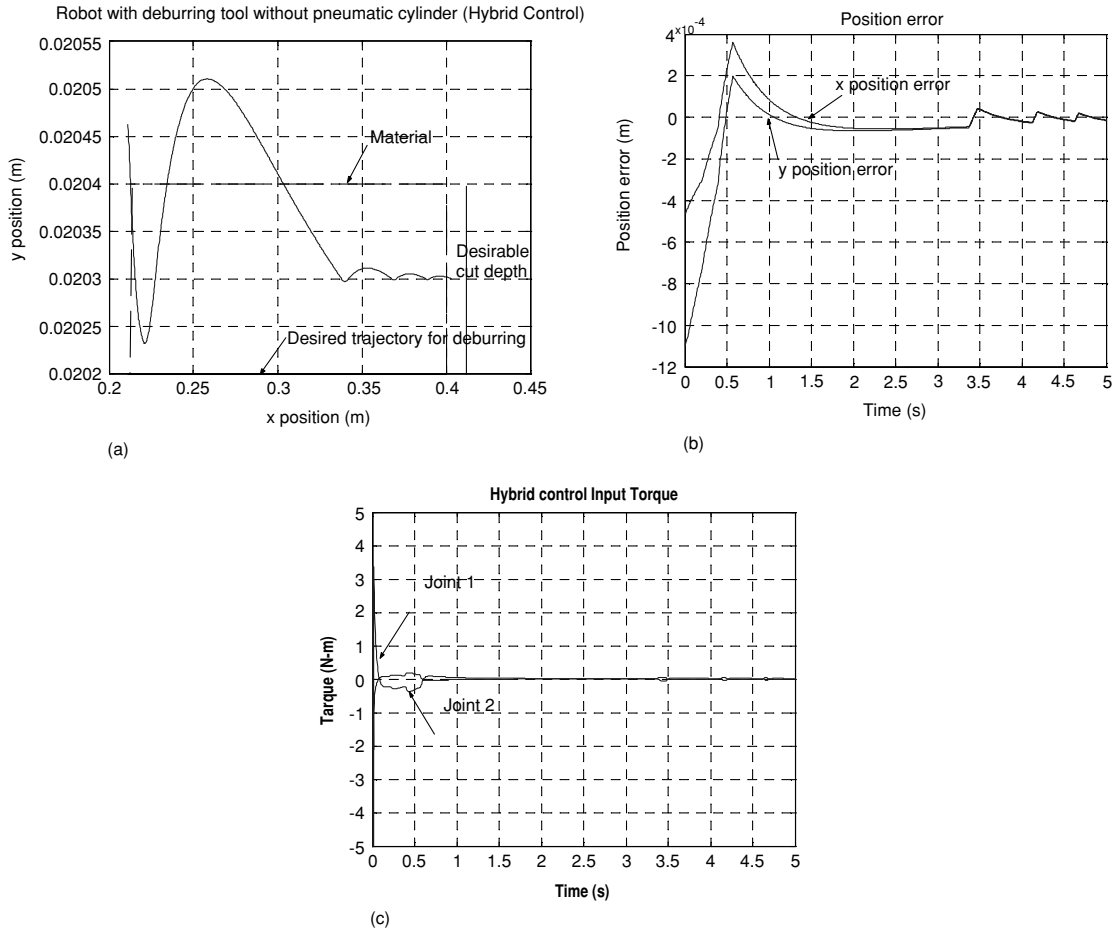

Fig. 6. Rigid tool (a) tracking (b) position error (c) control input.

https://doi.org/10.1017/S0263574705002067 Published online by Cambridge University Press

IV. SIMULATION

Simulation study was performed to investigate the performance of the controllers developed for the robotic deburring systems with different tools: (1) the hybrid controller for the rigid tool based system, as shown in Figure 5 (2), the coordination controller for the single active pneumatic tool (3) the coordination controller for the double active pneumatic tool based system.

Figure 6 shows the simulation results for the hybrid control system. The following parameters were used in simulation:

$$m_1 = 16\,\text{kg}, \quad m_2 = 12\,\text{kg}, \quad l_1 = 0.5\,\text{m}, \quad \text{and } l_2 = 0.7\,\text{m}.$$

The feedback gains of the controller were chosen as following:

$$f_d = 20N, \quad k_{p1} = \text{diag}[150, 150, 150], \quad k_{d1} = \text{diag}[70, 70, 70],$$
$$k_{p2} = \text{diag}[750, 750, 750], \text{ and } k_{d2} = \text{diag}[230, 230, 230]$$

where f_d is the desired force.

Figures 6 (a) and (b) show the performance of the hybrid controller designed for the deburring robot with a rigid tool. In the simulation, the stiffness of the material was set to 500000 N/m and the desired cut depth was chosen to be $0.0002\,m$. The results show large deburring error, which remains oscillatory after large overshoot in the transient period due to chattering caused by the air compressibility and the contact motion between the robot and the workpiece. Figure 6 (c) shows the input force. It is evident that relatively large overshoot and chattering still persist in the response. Note that Eq. (23) was used to obtain the normal force. The parameters in Eq. (23) are referred to the commercialized deburring tool as $b = 16\,mm$, $v_t = 0.08\,m/s$, and $V_t = 30,000\,RPM$.

Figure 7 depicts the deburring performance of the coordination controller designed for the robot with a single pneumatic tool. The following parameters were used for simulation:

$$P_{1i} = P_{2i} = 1 \times 10^5\,Pa, \quad A_1 = A_2 = 0.000256m^2,$$
$$M = 0.01\text{kg}, \quad T_{1i} = T_{2i} = 293^\circ K, \quad \text{and } X_0 = 0.07m.$$

As shown in Figure 7 (a) and (b), the transient performance is improved significantly with the single active pneumatic tool with the coordination controller in comparison to the previous case. However, the steady-state performance still remains unsatisfactory due to the chatter that appears in the response, which is caused by the compressibility of the air in the pneumatic cylinder and therefore requires repetitive

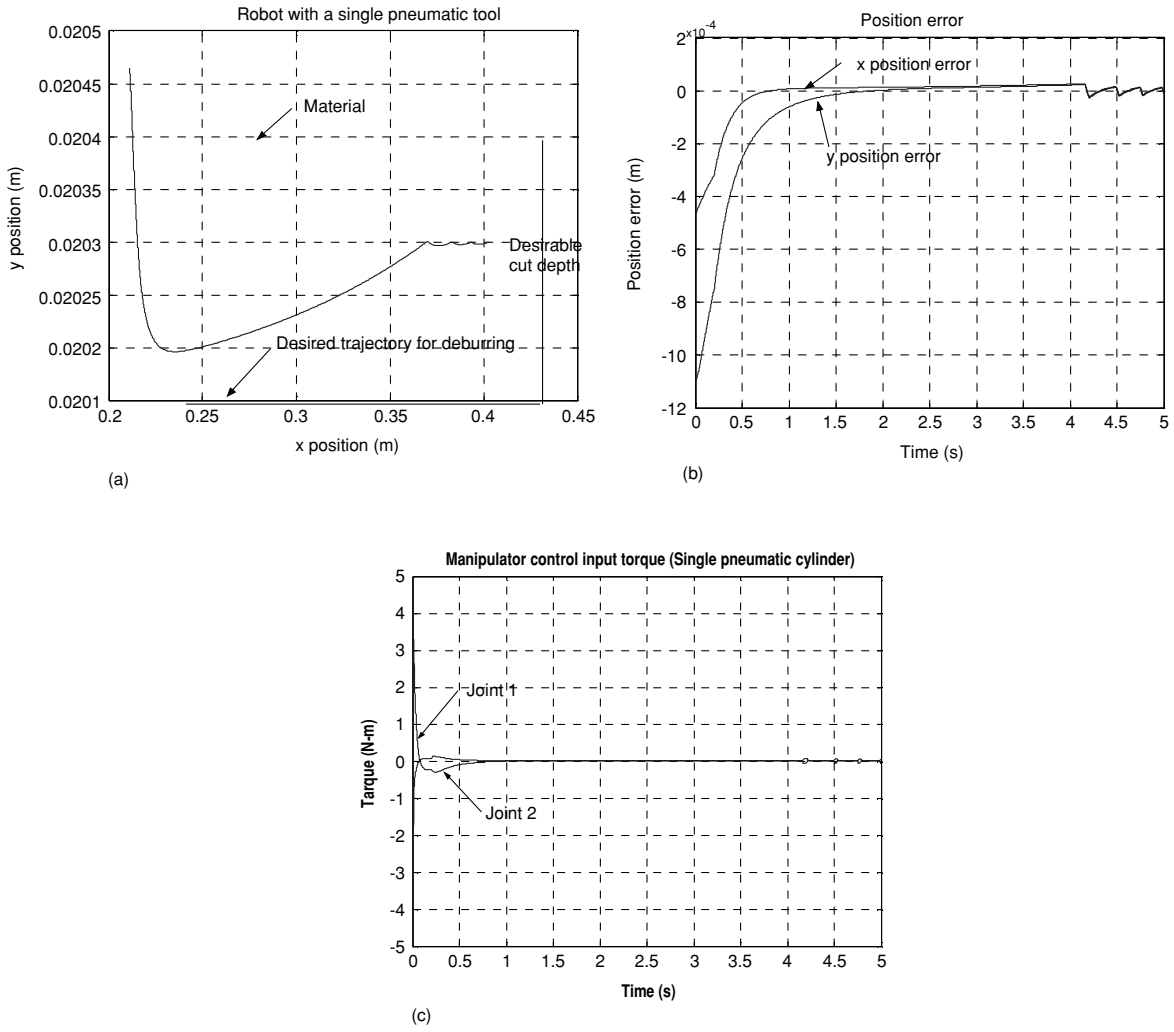

Fig. 7. Single pneumatic tool (a) tracking (b) position error(c) control input.

https://doi.org/10.1017/S0263574705002067 Published online by Cambridge University Press

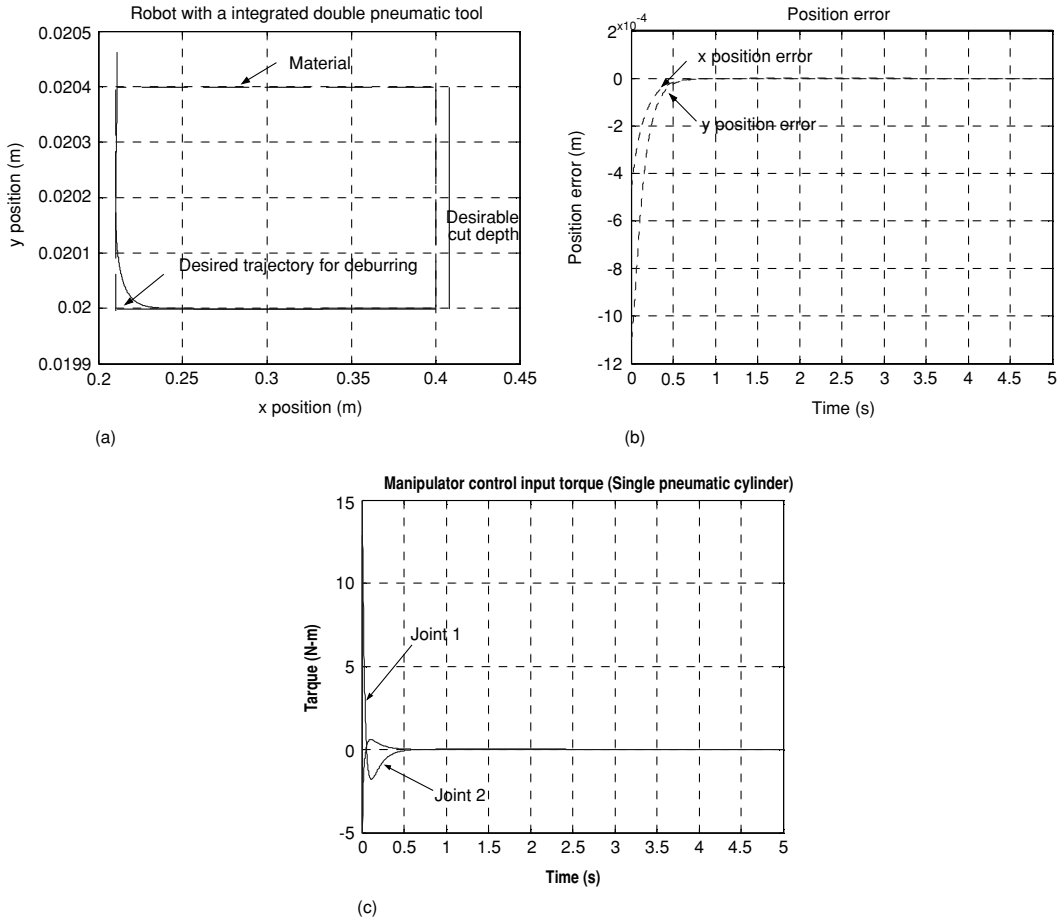

Fig. 8. Integrated double pneumatic cylinder (a) Tracking (b) position error (c) control input torque.

deburring. Nevertheless, the simulation results demonstrate the potential of a pneumatic actuator as an efficient tool which can significantly enhance the performance of a deburring robot if the chattering effect can be eliminated or minimized by an improved design of the tool and/or an efficient control.

Figure 8 demonstrates the deburring performance of the robot with the IPAS as shown in Figure 3. The developed coordination control method was utilized for the IPAS based deburring system. It is noted that the initial position of $M_i(i$=1, 2, 3, 4) is zero. The following is the additional parameters used for the integrated cylinder:

$$P_{3i} = 1 \times 10^5 Pa, \quad A_1 = A_2 = 0.000256m^2,$$
$$A_3 = 0.00055m^2, \quad n = 0.8, \quad F_{f1,2} = 10N,$$
$$F_{f3,4} = 15N, \quad M_{1,2} = 0.01\text{kg}, \quad M_{3,4} = 0.015\text{kg},$$
$$T_{1i} = T_{2i} = T_{3i} = 293^\circ K, \quad \text{and } x_0 = 0m.$$

It is evident as shown in Figure 8 (a) and (b) that the deburring performance of the system is greatly improved with the IPAS and the coordination controller. The simulation results show quick and smooth transient response and nearly zero steady-state error. The integrated system particularly improves the transient behavior in comparison to the double cylinder system. Figure 8 (c) depict the control input.

V. CONCLUSION

High-quality robotic deburring requires efficient control of the deburring path and contact forces, as well as optimal selection of a suitable feed-rate and tool design. In this paper, an efficient robotic deburring method was developed based on a new active pneumatic tool, which considers the interaction among the tool, the manipulator, and the workpiece and couples the tool dynamics and a control design that explicitly considers deburring process information. A new active pneumatic tool was developed by physically integrating two pneumatic actuators, which implements double cutting action – initial cut followed by fine cut. Then, a control method was developed for the robotic deburring system based on the active pneumatic tool, which utilizes coordination of two cutters. The developed control system employs the two-level hierarchical control structure based on a simple coordination scheme. Simulation results show that the developed system significantly reduces the chattering of the deburring robot and improves the deburring accuracy.

References

1. T. Furukawa, D. C. M. W. M. G. Dissanayake and A. J. Barratt, "Automated polishing of an unknown three-dimensional surface", *Robotics & Computer-Integrated Manufacturing* **12**, No. 3, 261–270 (1996).
2. T. R. Kurfess, D. E. Whitney and M. L. Brown, "Verification of a dynamic grinding model", *Journal of Dynamic Systems, Measurement and Control* **110**, No. 4, 403–409 (1988).

https://doi.org/10.1017/S0263574705002067 Published online by Cambridge University Press

3. M. W. Spong, F. L. Lewis and C. T. Abdallah, "Dynamics, motion planning,and analysis", *Robot Control* (IEEE Press, 1993), pp. 26–60.
4. D. E. Whitney, "Historical perspective and state of the art in robot force control", *Int. J. Robot. Res.* **6**, No. 1, 3–14 (1987).
5. T. Bopp, "Robotic finishing applications: Polishing sanding, grinding", *Proceeding of the 13 International Symposium on Industrial Robots* (1983), pp. 1–5.
6. N. Hogan, "Impedance control: An approach to manipulation: Part I, part II, part III", *ASME J. Dynam. Syst., Meas., Contr.*, **107**, 13–50 (1985).
7. N. Hogan, "Impedance control of industrial robots", *J. Robotics and Computer Integrated Manufacturing* **1**, No. 1, 97–113 (1984).
8. M. Cohen and T. Flash, "Learning Impedance Parameters for Robot Control using an Associative Search Network", *IEEE Transactions on Robotics and Automation* **7**, 382–390 (1991).
9. M. Raibert and J. Craig, "Hybrid position/force control of manipulators", *ASME J. Dyn. Syst., Meas., Contr.* **102**, 126–133 (1981).
10. O. Khatib, "A unified approach for motion and force control of robot manipulators: The operational space formulation", *IEEE J. Robotics Automat* **RA-3**, 43–53 (1987).
11. G. Duelen, H. Munch, D. Surdilovic and J. Timm, "Automated force control schemes for robotics deburring", *Proc. IEEE International Conference on Industrial Electronics, Control and Automation* (1992) Vol. 2, pp. 912–91.
12. M. H. Raibert and J. J. Craig, "Hybrid position/force control of manipulator", *ASME Journal of Dynamics System, Measurements and Control* **102**, 126–133 (1981).
13. M. W. Spong and M. Vidyasagar, *Robot Dynamics and Control* (1989), pp.141–150, and 247–251.
14. H. B. Kuntze, "On the closed-loop control of an elastic industrial robot", *Proc. American Control Conference* (1984) Vol. 3, pp. 1217–1223.
15. F. W. Paul, T. K. Gettys and J. D. Thomas, "Defining of iron castings using a robot positioned chipper", *Proc. ASME Robotics Research and Advanced Application* (1982), pp. 269–278.
16. A. Sharon and D. E. Hardt, "Enhancement of robot accuracy using endpoint feedback and a macro-micro manipulator system", *Proc. American Control Conference* (1984), pp. 1836–1844.
17. H. Asada and Y. Sawada, "Design of an adaptable tool guide for grinding robot", *Int. J. Robotics and Computer-Integrated Manufacturing* **2**(1), 49–54 (1985).
18. H. Asada and N. Goldfine, "Optimal compliance design for grinding robot tool holders", *IEEE Conference on Robotics and Automation* St. Louis, MO (1985), pp. 316–322.
19. H. Kazerooni and J. Guo, "Direct-drive, active compliant End-Effector", *IEEE Journal of Robotics and Automation* **4**, 130–175 (1987).
20. R. L. Hollis, "A planar XY robotic fine positioning device", *Proc. IEEE International Conference on Robotics and Automation* (1985), Vol. 2 pp. 329–336.
21. J. Wang, J. Pu, and P. R. Moore, "A practicable control strategy for servo pneumatic actuator systems", *Control Eng. Pract.* 1483–1488 (1997).
22. M. Sorli, L. Gastaldi, E. Codina and S. de las Heras, *Dynamic Analysis of Pneumatic Actuators Elsevier Science B. V.* (1999) 317–322.
23. S. Armstmstrong-Helouvry, P. Dupont, and C. Canudas De Wit, "A survey of models, analysis tools and compensation methods for the control of machines with friction", *Automatica* **30**(7), 1083–1183 (1994).
24. J. Deccusse and C. H. Moog, "Decoupling with dynamic compensation for strong invertible affine nonlinear systems", *International Journal of Control* **42**, 1387–1398 (1985).
25. A. Isidori, C. H. Moog, and A. De Luca, "A sufficient condition for full linearization via dynamic state feedback", *Proc. IEEE Conference on Decision and Control*, (Athens, Greece 1986), pp. 203–208.
26. Y. L. Chen, "Nonlinear feedback and computer control of robot arms", *Ph.D thesis*, Washington University, St. Louis, Missouri (1985), pp. 30–73.
27. A. Isidori, *Nonlinear Control Systems: An introduction*, (Springer Veriag. Berlin, New York, 1985), pp. 25–50.

https://doi.org/10.1017/S0263574705002067 Published online by Cambridge University Press